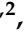



Article

Kinetic Constraints in the Specific Interaction between Phosphorylated Ubiquitin and Proteasomal Shuttle Factors

Ling-Yun Qin^{1,2}, Zhou Gong¹, Kan Liu¹ , Xu Dong^{1,*} and Chun Tang^{1,3,4,*} 

¹ Innovation Academy for Precision Measurement Science and Technology, Chinese Academy of Sciences, Wuhan 430071, China; qly_wh@wipm.ac.cn (L.-Y.Q.); gongzhou@wipm.ac.cn (Z.G.); liuk@apm.ac.cn (K.L.)

² University of Chinese Academy of Sciences, Beijing 100049, China

³ Beijing National Laboratory for Molecular Sciences, College of Chemistry and Molecular Engineering, Beijing 100871, China

⁴ Peking-Tsinghua Center for Life Sciences, Peking University, Beijing 100871, China

* Correspondence: dongxu@wipm.ac.cn (X.D.); Tang_Chun@pku.edu.cn (C.T.)

Abstract: Ubiquitin (Ub) specifically interacts with the Ub-associating domain (*UBA*) in a proteasomal shuttle factor, while the latter is involved in either proteasomal targeting or self-assembly coacervation. PINK1 phosphorylates Ub at S65 and makes Ub alternate between C-terminally relaxed (*pUb_{RL}*) and retracted conformations (*pUb_{RT}*). Using NMR spectroscopy, we show that *pUb_{RL}* but not *pUb_{RT}* preferentially interacts with the *UBA* from two proteasomal shuttle factors Ubqln2 and Rad23A. Yet discriminatorily, Ubqln2-*UBA* binds to *pUb* more tightly than Rad23A does and selectively enriches *pUb_{RL}* upon complex formation. Further, we determine the solution structure of the complex between Ubqln2-*UBA* and *pUb_{RL}* and uncover the thermodynamic basis for the stronger interaction. NMR kinetics analysis at different timescales further suggests an induced-fit binding mechanism for *pUb-UBA* interaction. Notably, at a relatively low saturation level, the dissociation rate of the *UBA-pUb_{RL}* complex is comparable with the exchange rate between *pUb_{RL}* and *pUb_{RT}*. Thus, a kinetic constraint would dictate the interaction between Ub and *UBA*, thus fine-tuning the functional state of the proteasomal shuttle factors.

Keywords: protein-protein interaction; ubiquitin; phosphorylation; proteasomal shuttle factor; ubiquitin-associated domain; induced fit



Citation: Qin, L.-Y.; Gong, Z.; Liu, K.; Dong, X.; Tang, C. Kinetic Constraints in the Specific Interaction between Phosphorylated Ubiquitin and Proteasomal Shuttle Factors.

Biomolecules **2021**, *11*, 1008. <https://doi.org/10.3390/biom11071008>

Academic Editor: Steven R. Van Doren

Received: 24 May 2021
Accepted: 7 July 2021
Published: 10 July 2021

Publisher's Note: MDPI stays neutral with regard to jurisdictional claims in published maps and institutional affiliations.



Copyright: © 2021 by the authors. Licensee MDPI, Basel, Switzerland. This article is an open access article distributed under the terms and conditions of the Creative Commons Attribution (CC BY) license (<https://creativecommons.org/licenses/by/4.0/>).

1. Introduction

The ubiquitin-proteasomal system is essential for maintaining proteostasis in the cell. Substrate proteins conjugated with the ubiquitin (Ub) chain in a particular manner can be targeted to the proteasome for degradation. The targeting process is mediated by the interactions between Ub and the intrinsic Ub receptors in the proteasome [1–3]. Ub-modified substrate proteins can also be targeted to the proteasome with the assistance of proteasomal shuttle factors. A shuttle factor contains an Ub-like domain (Ubl) at its N-terminus and one or more Ub-associating domains (*UBA*) at its C-terminus. The Ubl interacts with the same receptors in the proteasome, often with higher affinity than Ub [2,4]. The *UBA*, on the other hand, transiently interacts with Ub. Together, the proteasomal shuttle factor bridges the interaction between the substrate protein and the proteasome.

Ubiquitin-2 (Ubqln2) and Rad23A are the two common proteasomal shuttle factors. Ubqln2 is one of the four proteins, Ubqln1–4, in the ubiquitin family. Ubqln2 is prone to self-assembly to form liquid droplets or insoluble aggregates [5,6] and is associated with amyotrophic lateral sclerosis with frontotemporal dementia [7] and Huntington's disease [8]. On the other hand, the interaction with Ub via the Ubqln2-*UBA* domain can shift the equilibrium towards the diluted phase and dissipate Ubqln2 coacervate [5]. UV excision repair proteins, including Rad23A and Rad23B, can also phase separate in the cell. But unlike Ubqln2, Rad23 self-assembly is facilitated with the addition Ub chain, resulting

in the formation of proteasome foci in the cell [9]. The reason for the distinct coacervation behavior for the two proteasomal shuttle factors can be two-fold. First, a Rad23 protein harbors two tandem *UBA* domains, allowing multivalent interactions with Ub instead of just one *UBA* domain in Ubqln2. Second, Ub has a weaker binding for Rad23 than for Ubqln2 [10,11].

Ub not only modifies other proteins, Ub itself can also be modified [12]. Phosphorylation by kinase PINK1 at Ub residue S65 has been studied most intensively [13–15], thanks to its connection to the Parkinson's disease [16,17]. An increase of S65-phosphorylated Ub (*pUb*) level has been observed in neurons and brains of the aging population and neurodegenerative disease patients [18,19]. It has been suggested that Ub phosphorylation by PINK1 can inadvertently impair proteasomal activity and disrupt proteostasis [15]. Indeed, Ub phosphorylation can interfere with the synthesis and hydrolysis of the Ub chain [20–22], i.e., the writers and erasers of the Ub signaling cascade. In comparison, how Ub phosphorylation impacts the noncovalent interactions between Ub and other proteins is less clear [23]. A Ub phosphomimetic has been shown to bind to Rad23A much tighter than the wildtype Ub [21] in a quantitative proteomics study, but it is unknown how the wildtype *pUb* behaves.

When phosphorylated by PINK1 at S65, the resulting *pUb* can undergo a large conformational change to adopt a C-terminal retracted conformation (*pUb_{RT}*) [20]. The alternative conformation differs from the typical C-terminal relaxed conformation (*pUb_{RL}*), mainly in the hydrogen-bond register of the last β -strand (β 5). The two conformational states are in slow exchange and about equally populated at the physiological pH [14,24]. Importantly, mutants mimicking the S65 phosphorylation cannot elicit the alternative conformation [24,25]. To understand how the phosphorylation impacts Ub noncovalent interactions with other proteins, we characterized the binding dynamics and kinetics between *pUb* and the two *UBA* domains from Ubqln2 and Rad23A. Our results indicate that Rad23A does not bind to *pUb* more tightly than to Ub. Moreover, we show that Ubqln2-*UBA* selectively interacts with and enriches *pUb_{RL}* owing to a kinetic constraint.

2. Materials and Methods

2.1. Sample Preparation

Human ubiquitin was cloned to a pET11a vector and expressed in BL21 star cells. LB medium and M9-minimum medium were used to prepare unlabeled proteins and isotope-enriched proteins, respectively. Ubiquitin was purified through Sepharose SP and Sephacryl S100 columns (GE Healthcare, New Brunswick, NJ, USA) in tandem. For isotopic labeling, 1 g/L U-¹⁵N-labeled NH₄Cl (Isotec, Kürten, Germany) and/or 2 g/L U-¹³C-labeled glucose (Isotec, Milwaukee, WI, USA) were added to the M9-minimum medium as the sole nitrogen and/or carbon source.

PINK1 from body louse (phPINK1) was prepared as previously described [24]. To phosphorylate Ub, PINK1, Ub, MgCl₂, and ATP were mixed at the molar ratio of 1:10:500:500 in 20 mM Tris HCl buffer, also containing NaCl 150 mM, 1 mM DTT at pH 8.0. The reaction was performed at room temperature for 4 h. The *pUb* product was further purified with the Source Q column (GE Healthcare, New Brunswick, NJ, USA). Successful phosphorylation of Ub by PINK1 was confirmed by ESI mass spectrometry (Bruker Daltonics, Billerica, MA, USA).

The genes encoding the human Ubqln2-*UBA* (residues 578 to 621) and human Rad23A-*UBA2* (residues 315 to 363) were synthesized with optimized codons and sub-cloned into pET11a plasmid (a thioredoxin tag, a hexahistidine tag, and a TEV cleavage site were appended at the N-terminus of *UBA*). All proteins were expressed using BL21 (DE3) strain. LB medium and M9-minimal medium were used to prepare unlabeled and isotope-enriched proteins, respectively. After cell lysis, the protein was purified with a Ni-NTA agarose column (GE Healthcare, New Brunswick, NJ, USA) and a Sephacryl S100 column (GE Healthcare, New Brunswick, NJ, USA). The tags were removed with TEV protease at

4 °C overnight, followed by a second Ni-NTA agarose column (the desired protein was recovered in the flowthrough) and Sephacryl S100 columns column.

2.2. NMR Titration Experiments

For the titration of ^{15}N -labeled Ub or pUb with Ubqln2-UBA or Rad23A-UBA2, the initial NMR sample was prepared as 100 μM in 20 mM HEPES buffer (containing 150 mM NaCl at pH 7.4). A series of ^1H - ^{15}N HSQC spectra were recorded for the ^{15}N -labeled pUb sample with Ubqln2-UBA or Rad23A-UBA2 at 22.7 μM , 56.7 μM , 113.5 μM , 141.8 μM , 170.2 μM , 226.9 μM , 283.6 μM and 340.4 μM as the final concentration. The ^1H - ^{15}N HSQC spectra were recorded using a Bruker 600 MHz NMR spectrometer (Bruker Daltonics, Billerica, MA, USA) at 25 °C (298 K).

The NMR data were processed and analyzed using NMRPipe [26] and CCPNmr Analysis V2.4 [27], respectively. The CSPs were computed with $[0.5 \times \Delta\delta\text{H}^2 + 0.1 \times \Delta\delta\text{N}^2]^{0.5}$, in which $\Delta\delta\text{H}$ and $\Delta\delta\text{N}$ were the chemical shift difference in ^1H and ^{15}N dimensions, respectively.

2.3. Determination of K_D Value for pUb -UBA Complex

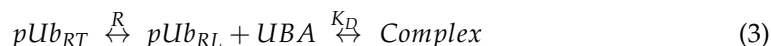
The zero-order equilibrium between pU_{RL} and pU_{RT} can be written as below:



The ratio between pUb_{RT} and pUb_{RL} concentrations is a constant at a particular pH [26]:

$$R = \frac{[pUb_{RT}]}{[pUb_{RL}]} \quad (2)$$

Now we consider the UBA interaction with pUb_{RL} , and the entire equilibrium can be written as follow:



The dissociation constant (K_D) between pUb_{RL} and UBA is defined as:

$$K_D = \frac{[pUb_{RL}^{free}] \times [UBA^{free}]}{[\text{Complex}]} \quad (4)$$

The total concentration of pUb [M] is:

$$M = [pUb_{RT}] + [pUb_{RL}^{free}] + [\text{Complex}] \quad (5)$$

The concentration of UBA added [T] at a given titration point is known and can be substituted in the following equation:

$$M = [pUb_{RT}] + \frac{[pUb_{RT}]}{R} + [T] - [UBA^{free}] \quad (6)$$

$$pUb_{RL}^{free} = \frac{[pUb_{RT}]}{R} = \frac{K_D \times ([T] - [UBA^{free}])}{[UBA^{free}]} \quad (7)$$

Combining Equations (6) and (7), the $[pUb_{RT}]$ is described as follow:

$$[pUb_{RT}] = \frac{-\{R \times ([T] - M) + K_D \times R \times (R+1)\} + \sqrt{\{R \times ([T] - M) + K_D \times R \times (R+1)\}^2 + 4 \times M \times R^2 \times K_D \times (1+R)}}{2 \times (R+1)} \quad (8)$$

On the other hand, the sum of $[pUb_{RL}]$ and the concentration of pUb_{RL} in the complex form is defined in the following equation:

$$[P] = [pUb_{RL}^{free}] + [\text{Complex}] = M - \frac{-\{R \times ([T] - M) + K_D \times R \times (R+1)\} + \sqrt{\{R \times ([T] - M) + K_D \times R \times (R+1)\}^2 + 4 \times M \times R^2 \times K_D \times (1+R)}}{2 \times (R+1)} \quad (9)$$

For NMR titration, the relationship between the CSP and protein concentration is described as follow:

$$\delta_{obs} = \delta_{min} + n \times (\delta_{max} - \delta_{min}) \times \frac{\left([T] + \frac{[P]}{n} + K_D\right) - \sqrt{\left([T] + \frac{[P]}{n} + K_D\right)^2 - \frac{4 \times [T] \times [P]}{n}}}{2 \times [P]} \quad (10)$$

in which δ_{obs} is the observed CSP value at a given titration point, n is the stoichiometric ratio, $[P]$ is the total concentration of pUb relaxed state, δ_{min} is the minimum value of CSP, δ_{max} is the maximal value of CSP. $[T]$ is the concentration of the UBA domain. In Equation (10), $[P]$ is described using Equation (9), the value of K_D for the complex between UBA and pUb relaxed state could be calculated by fitting the concentration of UBA $[T]$ against observed CSP δ_{obs} .

2.4. CPMG Relaxation Dispersion Experiment

^{15}N -edited CPMG measurement was performed for the NMR sample of the complex between Ubqln2- UBA and pUb prepared as concentrations (in 150 mM NaCl, 20 mM HEPES pH 7.4 buffer); one with 32 μM pUb and 300 μM Ubqln2 UBA (~10% saturation), and the other with 228 μM pUb and 300 μM Ubqln2 UBA (~50% saturation). The complex samples of Rad23A- $UBA2$ and pUb were also prepared with 54 μM pUb and 300 μM Rad23A- $UBA2$ (~5% saturation). The NMR sample of the complex between Ubqln2- UBA and ^{15}N - pUb prepared as concentrations (in 20 mM HEPES pH 7.4 buffer with 150 mM NaCl); one with 39 μM Ubqln2 UBA and 300 μM ^{15}N - pUb (~10% saturation), and the other with 229 μM Ubqln2 UBA and 300 μM ^{15}N - pUb (~50% saturation). The CPMG experiments were recorded using Bruker 600 MHz, 700 MHz, and 850 MHz NMR spectrometers (Bruker Daltonics, Billerica, MA, USA) using the standard pulse sequence [28]. The CPMG spin-echo pulsing frequency includes 0 Hz, 40 Hz, 120 Hz, 200 Hz, 280 Hz, 360 Hz, 600 Hz, and 760 Hz. The NMR data were processed using NMRPipe and fitted using Glove [29].

The concentration of the free pUb_{RL} can be calculated using Equations (2) and (4). The relationship between K_D , k_{ex} , k_{on} , and k_{off} is described in Equations (11) and (12), and thus can be calculated.

$$k_{ex} = k_{on} \times [pUb_{RL}^{free}] + k_{off} \quad (11)$$

$$K_D = \frac{k_{off}}{k_{on}} \quad (12)$$

2.5. Acquisition of NMR ZZ-Exchange Data

^{15}N -labeled pUb (380 μM) and Ubqln2- UBA (280 μM) were mixed in 20 mM HEPES buffer at pH 7.4 containing 150 mM NaCl. As a control, 380 μM free ^{15}N -labeled pUb was prepared in the HEPES buffer. The experiments were performed on a Bruker 600 MHz NMR spectrometer (Bruker Daltonics, Billerica, MA, USA) at 30 °C. The delay times for the ZZ-exchange were set at 0 ms, 20 ms, 40 ms, 60 ms, 90 ms, 120 ms, 160 ms, 220 ms, 380 ms, and 450 ms. The signal intensities with different delays were evaluated and used to fit the exchange rates between pUb_{RL} and pUb_{RT} , using the established method [30].

2.6. Calculation of the UBA - pUb Complex Structure

The ^{13}C -edited F1-filtered NOESY spectra were recorded with a 120 ms mixing time on a 600 MHz NMR spectrometer at 25 °C. The $^{15}\text{N}/^{13}\text{C}$ -labeled Ubqln2- UBA (500 μM) and pUb (750 μM) were mixed in 20 mM HEPES buffer pH 7.4 with NaCl 150 mM. For the RDC sample, ^{15}N -labeled pUb (300 μM) and Ubqln2 UBA (700 μM) were mixed in the same buffer. Residual dipolar couplings (RDC) were recorded for backbone amide bond vectors in PEG (C_{12}E_5)/hexanol (6%; Sigma-Aldrich, Saint-Louis, MO, USA) alignment medium [31], using the in-phase/anti-phase scheme.

The structure of the complex between the Ubqln2 UBA and the pUb_{RL} was calculated using XPLOR-NIH [32]. The topology and parameter files for phosphorylated serine (SEP) were generated as previously described [14]. For the intra-molecular restraints of Ubqln2

UBA (PDB code: 2JY6) and the *pUb* relaxed state (PDB code: 5XK5), the published data were used during the structure determination [24]. Intermolecular NOE and RDC restraints were used to restrain the complex structure. The RDC restraints of *pUb_{RL}* with Ubqln2-*UBA* (85% complex at *pUb* and Ubqln2-*UBA* concentrations of 300 μ M) and its free form were recorded separately in the same alignment medium. To determine the RDC values of *pUb_{RL}*/Ubqln2 *UBA* complex, the contribution of the free form of *pUb_{RL}* was subtracted from the observed data of the sample of *pUb_{RL}* with Ubqln2 *UBA*, using the following equation:

$$RDC_{complex} = \frac{(RDC_{complex-measured} - RDC_{free-measured} \times \%free)}{\%complex} \quad (13)$$

Two hundred forty structures each were calculated, and the top-ranked 20 structures with the lowest energy were selected. The structures were further subjected to water refinement. for further analysis. Structure figures were rendered using PyMOL Version 2.2 (The PyMOL Molecular Graphics System, Schrödinger). The complex structure of Ubqln2-*UBA* and *pUb_{RL}* has been deposited at the PDB with the accession number of 7F7X.

3. Results

3.1. *UBA* Selectively Interacts with *pUb_{RL}*

We titrated the unlabeled *UBA* domain from Ubqln2 or the second *UBA* domain (*UBA2*) from Rad23A to 15 N-labeled *pUb*. The titration causes progressive chemical shift perturbations (CSPs) for a subset of peaks in *pUb_{RL}* but almost negligible CSPs for the peaks corresponding to *pUb_{RT}*. Though the CSP magnitude is similar for *pUb_{RL}* when titrated with two *UBA* domains, the largest perturbed residues are found in $\beta 4$ and $\beta 2$ with the Ubqln2-*UBA* $\beta 5$ and with the Rad23A-*UBA2* (Figure 1).

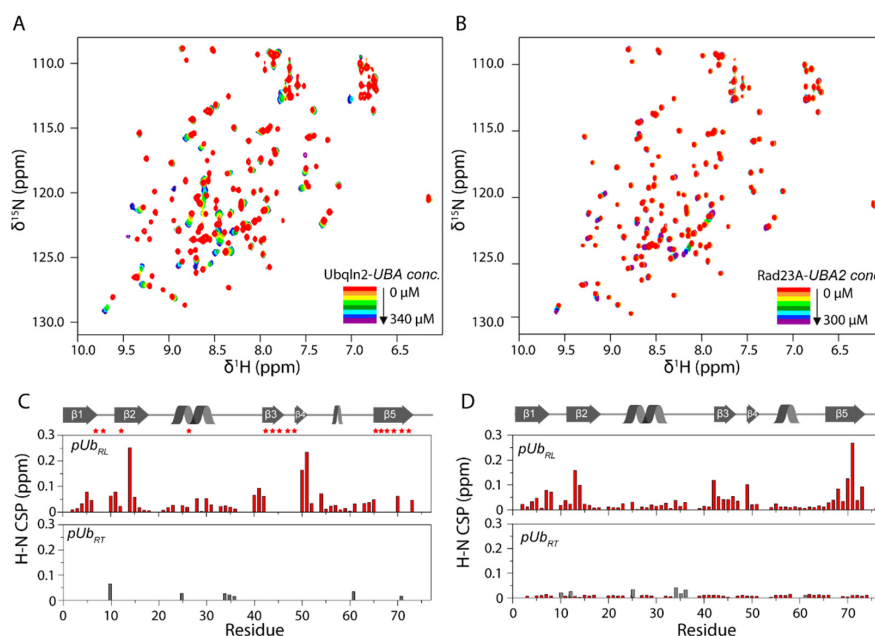


Figure 1. NMR titrations show that Ubqln2-*UBA* and Rad23A-*UBA2* selectively interact with *pUb_{RL}*. (A,B) A series of ^1H - ^{15}N HSQC were recorded to monitor the amide chemical shift changes upon titration of Ubqln2-*UBA* and Rad23A-*UBA2*, respectively, and the spectra for different titration points are colored like a rainbow. (C,D) Chemical shift perturbations (CSPs) for the backbone amide of 100 μM ^{15}N -labeled *pUb_{RL}* and *pUb_{RT}* upon titration of 340 μM Ubqln2-*UBA* and 300 μM Rad23A-*UBA2*, with the secondary structure of *pUb* shown as a cartoon. The amide signals that disappear in the complex are indicated with asterisks. The gray columns indicate the residues of *pUb_{RL}* and *pUb_{RT}* have the same chemical shifts.

Ubqln2-UBA not only selectively interacts with pUb_{RL} and also enriches pUb_{RL} to nearly 100%. When binding to Ubqln2-UBA, pUb undergoes a further equilibrium shift from pUb_{RT} to pUb_{RL} . In comparison, the addition of Rad23A-UBA2 causes little populational change for the pUb , even with the addition of a very high concentration (Figure 2).

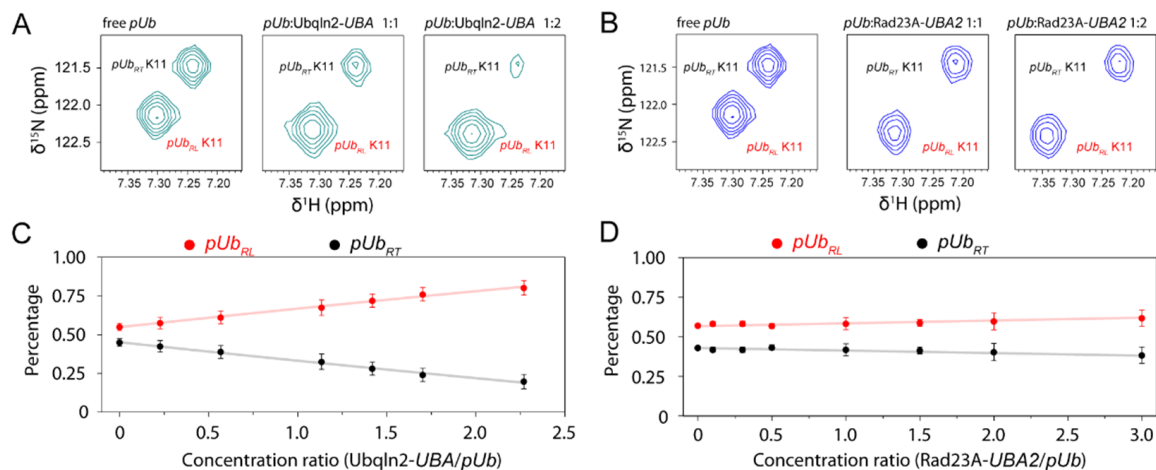


Figure 2. NMR titrations show that Ubqln2-UBA selectively enriches pUb_{RL} at the expense of pUb_{RT} . The zoomed-in view of ^1H - ^{15}N HSQC shows the peaks of K11 of pUb_{RL} and pUb_{RT} at the different molar ratio with Ubqln2-UBA (A) and Rad23A-UBA2 (B). (C,D) The populations of pUb_{RL} (red) and pUb_{RT} (black) are extracted from the titration of Ubqln2-UBA and Rad23A-UBA2. The values are calculated as the percentages of the peak volume of the pUb conformational state over the combined peak volume of both pUb states, averaged for four residues at the Ub-UBA interface; the error bar indicates one standard deviation. The plot shows that the population of pUb_{RL} increases upon the addition of Ubqln2-UBA but barely changes upon the addition of Rad23A-UBA2.

In the standard one-site binding isotherm model, the concentration of the titrated protein is fixed. In a previous study by Fushman and coworkers, the titration points between pUb and the UBA domain from Ubqln1, a close homolog of Ubqln2 in the same family, were fitted with a simple one-site binding curve [25]. However, systematic deviations can be noticed from the fitting (Figure S1). Upon UBA titration, the total pUb_{RL} concentration changes, while the unbound pUb_{RL} concentration should maintain a constant ratio with the pUb_{RT} concentration. Thus, a revised model is needed to account for the coupled equilibria of the interconversion between pUb_{RL} and pUb_{RT} and the interaction between pUb_{RL} and UBA, as described in the Methods section. Using this model, we obtained the K_D values of $43.3 \pm 3.6 \mu\text{M}$ and $403.5 \pm 38.8 \mu\text{M}$ for Ubqln2-UBA and Rad23A-UBA2, respectively (Figure 3A,C). Notably, the residuals are small and random from the fittings (Figure S2).

As a control, we performed titrations of Ubqln2-UBA and Rad23A-UBA2 to ^{15}N -labeled unmodified Ub. The K_D values are $33.0 \pm 3.7 \mu\text{M}$ and $355.8 \pm 56.0 \mu\text{M}$ for Ubqln2-UBA and Rad23A-UBA2, respectively. Thus, phosphorylation only slightly decreases the binding affinities of the UBA towards the pUb_{RL} (Figure 3B,D).

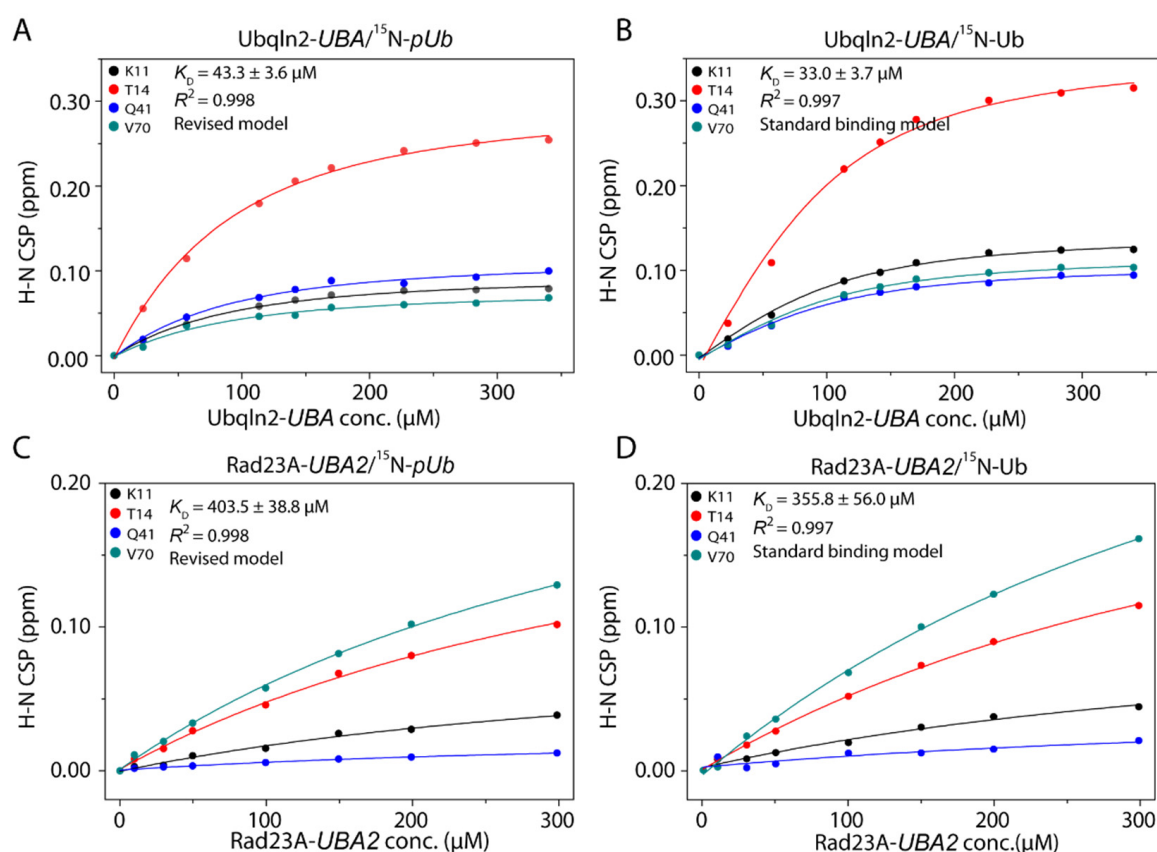


Figure 3. Fitting of the binding equilibrium constants between *UBA* and *pUb_{RL}* using our revised model. The interfacial residues were selected for their largest and continuously visible CSPs. (A,C) Fitting the CSPs of ¹⁵N-labeled *pUb* upon the titration of *Ubqln2-UBA* and *Rad23A-UBA2*. The K_D values are $43.3 \pm 3.6 \mu\text{M}$ and $403.5 \pm 38.8 \mu\text{M}$, respectively. (B,D) Fitting the CSPs of ¹⁵N-labeled *Ub* upon the titration of *Ubqln2-UBA* and *Rad23A-UBA2* using a simple one-site binding model. The K_D values are $33.0 \pm 3.7 \mu\text{M}$ and $355.8 \pm 56.0 \mu\text{M}$, respectively.

3.2. The Complex Structure Explains the Binding Preference for *Ubqln2-UBA*

We collected the intermolecular NOEs between *pUb* and *Ubqln2-UBA* using a filtered/edited NMR pulse sequence. Consistent with the titration results, the NOE cross-peaks were only identified between the resonances associated with *pUb_{RL}* and the resonances in *Ubqln2-UBA* (Figure S3, Table S1). On the other hand, we could not observe intermolecular NOEs between *pUb* and *Rad23A-UBA2*. The failure to produce intermolecular NOEs can be explained by the short lifetime, i.e., fast dissociation rate, of the *Rad23A-pUb* complex, as will be discussed below. In addition to the NOEs, experimental restraints also include residual dipolar couplings (RDCs), measured for each subunit at an exact complex occupancy.

The structure of the complex between *pUb_{RL}* and *Ubqln2-UBA* is well-converged with the root-mean-square deviations for all backbone heavy atoms of $0.81 \pm 0.09 \text{ \AA}$ (Figure S4 and Table S2). The structure is similar to those determined for other *UBA-Ub* complexes [11,33]. Formation of the complex buries solvent-accessible surface area of $1022.7 \pm 139.7 \text{ \AA}^2$, which involves hydrophobic residues of L8, I44, and V70 in *pUb_{RL}* and hydrophobic residues I611 and I615 in *Ubqln2-UBA* (Figure 4A). Moreover, the β -sheet slightly bends upon complex formation, as the distance between the $C\beta$ atoms of residues I44 and V70 is shortened from $6.3 \pm 0.2 \text{ \AA}$ in the free *pUb_{RL}* to $5.8 \pm 0.2 \text{ \AA}$ in the *UBA*-bound *pUb_{RL}*. Since $\beta 5$ moves up by two residues in *pUb_{RT}* [20,24], the interaction between V70 in *pUb_{RL}* and I615 in *Ubqln2-UBA* would be abolished. This explains why the *UBA* selectively interacts with *pUb_{RL}*.

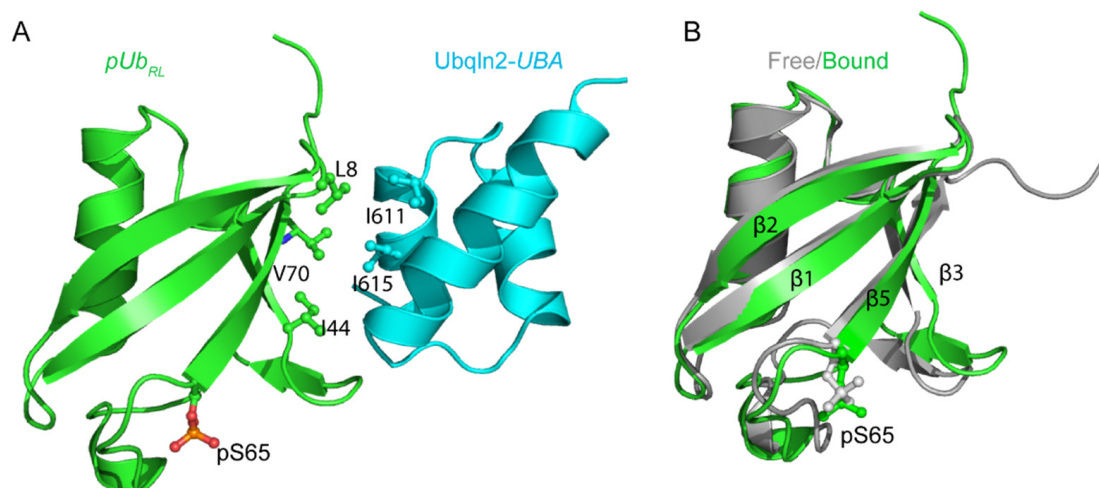


Figure 4. Solution structure of pUb_{RL} in complex with Ubqln2-UBA (PDB code: 7F7X, this study). (A) The structure of the complex between Ubqln2-UBA (cyan) and pUb_{RL} (green), with the pS65 sidechain shown as sticks. The key interfacial residues, including L8, I44, and V70 in pUb_{RL} , and I611 and I615 in Ubqln2-UBA are also shown. (B) Superposition of pUb_{RL} structure in the free form (gray) or complex with Ubqln2-UBA (green). The pS65 sidechains are shown as sticks.

The phosphorylated residue pS65 is located outside the interface between pUb_{RL} and Ubqln2-UBA. This explains why Ubqln2-UBA binds to pUb_{RL} only slightly weaker than the unmodified Ub (Figure 4A). Interestingly, the interface does not involve residues in $\beta 2$. Therefore, the observed CSP for $\beta 2$ residues (Figure 1) is likely caused by the allosteric modulation of the β -sheet structure upon Ubqln2-UBA binding. Indeed, significant changes in the RDC values are observed for the interfacial residues and the backbone N-H bond vector of $\beta 2$ residue L15 (Figure S5). As a result, $\beta 1$ and $\beta 2$ strands curl slightly in the UBA complex (Figure 4B).

Rad23A-UBA2 is highly homologous to Ubqln2-UBA. However, the interfacial residues I611 and I615 in Ubqln2-UBA are substituted with glutamate and alanine residues, respectively, in Rad23A-UBA2. Therefore, Rad23A-UBA2 interacts with pUb_{RL} much weaker than Ubqln2-UBA. Moreover, Rad23A-UBA2 likely adopts a slightly different conformation in the complex, which would explain the different CSP profile (Figure 1).

3.3. Kinetic Constraints for pUb Interaction

The addition of Ubqln2-UBA enriches pUb_{RL} . However, the addition of Rad23-UBA largely failed to promote pUb conformational conversion. To account for the different selectivity for the UBA domain, we performed a detailed kinetics analysis during the formation of the pUb -UBA complex.

We first performed CPMG relaxation dispersion measurement for ^{15}N -labeled Ubqln2-UBA, with the unlabeled pUb added to $\sim 10\%$ and $\sim 50\%$ saturation of the complex (Figure 5). The measurements were performed at two different magnetic fields, and the k_{ex} values for the exchange rate between free and bound proteins can be obtained in a global fit. At $1382.9 \pm 3.7 \text{ s}^{-1}$ and $320.3 \pm 13.9 \text{ s}^{-1}$, the k_{ex} value is nearly four times larger at the higher concentration level. Using the k_{ex} values and the K_D value (the zero-order interconversion equilibrium constant between pUb_{RL} and pUb_{RT} is set to 0.67), we obtained the concentration of the unbound pUb_{RL} and determined the k_{on} and k_{off} values— $6.8 \pm 0.6 \mu\text{M}^{-1} \text{ s}^{-1}$ and $293.1 \pm 27.5 \text{ s}^{-1}$ at the low saturation level, and $15.6 \pm 1.4 \mu\text{M}^{-1} \text{ s}^{-1}$ and $677.8 \pm 61.0 \text{ s}^{-1}$ at the high saturation level.

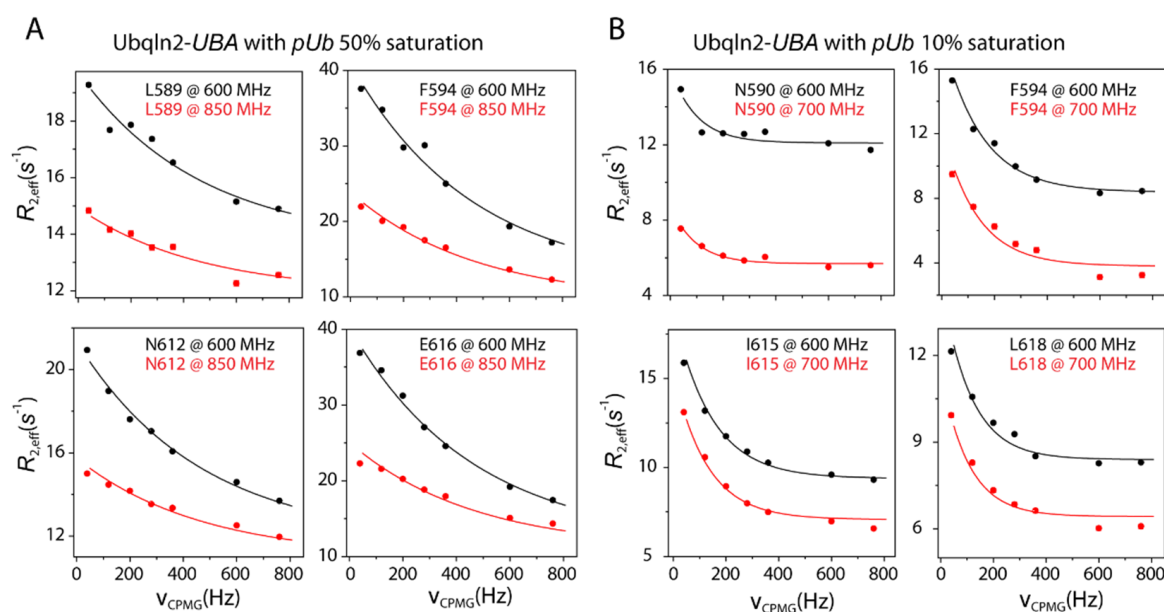


Figure 5. CPMG relaxation dispersion analysis for ^{15}N -labeled Ubqln2-UBA at two different magnetic fields. The unlabeled *pUb* was added to $\sim 10\%$ and $\sim 50\%$ saturation. Experimental values of $R_{2,\text{eff}}$ at different CPMG frequencies are shown as dots, with the error bar indicates one standard deviation in the measurement.

Reciprocally, we performed CPMG relaxation dispersion measurements for ^{15}N -labeled *pUb*, with the unlabeled Ubqln2-UBA added at $\sim 10\%$ or $\sim 50\%$ saturation. However, the fitting was poor, especially at 10% saturation. We managed to obtain the k_{ex} value using residue L71 in the *pUb_{RL}* conformational state (Figure S6A,B), and the exchange rate at 50% saturation is also much higher than that at 10% saturation. As a control, we performed CPMG relaxation dispersion measurement for ^{15}N -labeled *pUb* alone. The change in the ^{15}N R_2 value for L71 in the free *pUb* is negligible, indicating a lack of μs -ms timescale, which has been noted for the unmodified Ub [34].

Binding to Ubqln2-UBA also perturbs the exchange dynamics between *pUb_{RL}* and *pUb_{RT}*. The interconversion between the two Ub states occurs at ms-s timescale and can be probed with ZZ-exchange spectroscopy [20]. Binding to Ubqln2-UBA causes slight retardation of the back exchange from *pUb_{RL}* to *pUb_{RT}* compared to the free *pUb* (Figure S7).

We also performed CPMG relaxation dispersion measurements for the ^{15}N -labeled Rad23-UBA2 with the unlabeled *pUb* added to $\sim 5\%$ saturation. The ^{15}N R_2 values only decreases slightly at an increasing CPMG pulsing frequency (Figure S8). Thus, only a lower limit could be estimated for the k_{ex} value for the exchange rate between free and bound forms, which is $\sim 40,000 \text{ s}^{-1}$.

4. Discussion

Ub is an important signaling molecule and performs its function by modifying other proteins, the post-translational modification process known as ubiquitination. Discoveries made in the past ten years have shown that Ub itself can be modified, and Ub modifications can profoundly remodel Ub signaling [12,15]. Ub is phosphorylated at residue S65 by PINK1 [13]. The *pUb* slowly interconverts between two distinct conformational states, namely *pUb_{RL}* and *pUb_{RT}* [20]. Using NMR titrations, we have shown that the UBA from Ubqln2 and Rad23A selectively interacts with *pUb_{RL}* but not *pUb_{RT}*. We have thus characterized the complex structure between Ubqln2-UBA and *pUb_{RL}* and provided an atomic explanation for the UBA selectivity of the particular *pUb* state. Interestingly, Ubqln2-UBA selectively enriches *pUb_{RL}* at the expense of *pUb_{RT}* during the interaction. Prompted by this finding, we revised the one-site binding model to account for the changing concentration of *pUb_{RL}* during UBA titration. The K_D values from the fitting show that thermodynamically, the UBA binding to *pUb_{RL}* is only slightly weaker than to the unmodified Ub. This is

consistent with the fact that pUb_{RL} and Ub are structurally similar, and the phosphorylated residue is away from the binding interface (Figure 4).

The selective enrichment of pUb_{RL} by Ubqln2-UBA not only has to do with the thermodynamics of the binding equilibrium but has to do with the association/dissociation kinetics. The interconversion between the free and bound forms for Ubqln2 complex is much slower than that for the Rad23A complex. A slower off-rate means a longer lifetime for the Ubqln2- pUb complex, allowing intermolecular NOEs to build up (Figure S3). The slower interconversion rate also means that Ubqln2-UBA is more capable, kinetically, of driving the conversion from pUb_{RT} to pUb_{RL} .

However, the experimentally determined k_{on} and k_{off} rates of the Ubqln2- pUb complex are larger than the interconversion timescale between pUb_{RT} and pUb_{RL} by over an order of magnitude. Interestingly, the k_{on} and k_{off} rates decrease when the saturation level of the complex is lower. Upon extrapolation, the k_{off} rate would be even lower at the start of the binding process, comparable to the timescale of pUb_{RT}/pUb_{RL} interconversion. Moreover, upon Ubqln2 binding, the back conversion from pUb_{RL} to pUb_{RT} is slightly slowed (Figure S7). Together, owing to the kinetic constraint, pUb_{RL} can be efficiently enriched by Ubqln2 but not by Rad23A.

The acceleration of the binding kinetics at higher complex occupancy can be explained by the conformational restriction of pUb_{RL} . Ub undergoes a so-called pincer-like movement, with the residues in $\beta 1$ and $\beta 2$ experience large fluctuation at sub- μs timescale [35,36]. The association of a UBA stabilizes one of the preexisting conformations of the β -sheet structure. However, Ub does not simply bind to UBA through conformational selection; an induced fit or conformational restriction mechanism also plays an important role in the interaction between Ub and its partner protein, especially towards the end of the binding process [37,38]. The increased exchange rate between free and bound proteins at an increasing saturation level of the complex is characteristic of an induced-fit mechanism [39]. Microscopically, the interaction with Ubqln2-UBA induces and stabilizes a UBA-complementary conformation of pUb_{RL} (Figure 4), which would permit rapid association and dissociation. In a sense, Ub phosphorylation by PINK1 can be likened to Ub mutations specifically introduced that ultimately drive the Ub-binding mechanism to induced fit [40]. Nevertheless, a precise dissection of the two binding mechanisms warrants further analysis [41,42].

As such, phosphorylation at Ub residue S65 provides additional kinetic and dynamic constraints for Ub-UBA noncovalent interactions, which would determine whether the proteasomal shuttle factor remains monomeric for proteasomal targeting or phase-separate to form liquid or solid coacervate.

Supplementary Materials: The following are available online at <https://www.mdpi.com/article/10.3390/biom11071008/s1>, Figure S1: Reanalysis of the NMR titration data between pUb and the UBA domain of ubiquilin1, published by Fushman and coworkers [25]; Figure S2: (A,C) The residuals from the fitting the CSPs of ^{15}N -labeled pUb upon UBA titration, using the revised model, related to Figure 3A,C. (B,D) The residuals from the fitting the CSPs of ^{15}N -labeled Ub upon UBA titration, using the simple one-site binding model, related to Figure 3B,D; Figure S3: Intermolecular NOEs identified between $^{13}C,^{15}N$ -labeled Ubqln2-UBA and unlabeled pUb_{RL} ; Figure S4: Superposition of the 20 lowest-energy conformers calculated for Ubqln2-UBA (cyan) and pUb_{RL} complex (green), shown in two perspectives; Figure S5: Comparison between observed and calculated RDC values for pUb_{RL} ; Figure S6: CPMG relaxation dispersion measurements were performed for ^{15}N -labeled pUb at two different magnetic fields; Figure S7: The interconversion rate between pUb_{RL} and pUb_{RT} analyzed with NMR ZZ-exchange experiment; Figure S8: CPMG relaxation dispersion measurements performed for ^{15}N -labeled Rad23A-UBA2 at 600 MHz with the unlabeled pUb added to ~5% saturation; Table S1: Intermolecular distance restraints for the structure calculation of Ubqln2-UBA/ pUb_{RL} complex.; Table S2: Structure statistics for the Ubqln2-UBA/ pUb_{RL} complex; Table S3: The fitted values of k_{ex} , k_{on} , and k_{off} of pUb_{RL} /Ubqln2 UBA complex.

Author Contributions: Conceptualization, C.T.; methodology, K.L. and Z.G.; formal analysis, L.-Y.Q., X.D. and Z.G.; data curation, L.-Y.Q. and X.D.; writing—original draft preparation, L.-Y.Q. and X.D.; writing—review and editing, C.T.; supervision, X.D. and C.T.; funding acquisition, X.D. and C.T. All authors have read and agreed to the published version of the manuscript.

Funding: The work has been supported by the National Key R&D Program of China (2018YFA0507700, 2017YFA0505400, and 2016YFA0501200) and by the National Natural Science Foundation of China (31770799, 21921004, and 31971155).

Institutional Review Board Statement: Not applicable.

Informed Consent Statement: Not applicable.

Data Availability Statement: The data have been deposited with the PDB and BMRB with the accession codes of 7F7X and 36427, respectively.

Conflicts of Interest: The authors declare no conflict of interest.

References

- Schreiner, P.; Chen, X.; Husnjak, K.; Randles, L.; Zhang, N.X.; Elsassner, S.; Finley, D.; Dikic, I.; Walters, K.J.; Groll, M. Ubiquitin docking at the proteasome through a novel pleckstrin-homology domain interaction. *Nature* **2008**, *453*, 548–552. [[CrossRef](#)]
- Shi, Y.; Chen, X.; Elsassner, S.; Stocks, B.B.; Tian, G.; Lee, B.H.; Shi, Y.; Zhang, N.; de Poot, S.A.; Tuebing, F.; et al. Rpn1 provides adjacent receptor sites for substrate binding and deubiquitination by the proteasome. *Science* **2016**, *351*, aad9421. [[CrossRef](#)]
- Liu, Z.; Dong, X.; Yi, H.W.; Yang, J.; Gong, Z.; Wang, Y.; Liu, K.; Zhang, W.P.; Tang, C. Structural basis for the recognition of K48-linked Ub chain by proteasomal receptor Rpn13. *Cell Discov.* **2019**, *5*, 19. [[CrossRef](#)] [[PubMed](#)]
- Chen, X.; Ebelle, D.L.; Wright, B.J.; Sridharan, V.; Hooper, E.; Walters, K.J. Structure of hRpn10 Bound to UBQLN2 UBL Illustrates Basis for Complementarity between Shuttle Factors and Substrates at the Proteasome. *J. Mol. Biol.* **2019**, *431*, 939–955. [[CrossRef](#)]
- Dao, T.P.; Kolaitis, R.M.; Kim, H.J.; O'Donovan, K.; Martyniak, B.; Colicino, E.; Hehnl, H.; Taylor, J.P.; Castaneda, C.A. Ubiquitin Modulates Liquid-Liquid Phase Separation of UBQLN2 via Disruption of Multivalent Interactions. *Mol. Cell* **2018**, *69*, 965–978 e966. [[CrossRef](#)]
- Sharkey, L.M.; Safren, N.; Pithadia, A.S.; Gerson, J.E.; Dulchavsky, M.; Fischer, S.; Patel, R.; Lantis, G.; Ashraf, N.; Kim, J.H.; et al. Mutant UBQLN2 promotes toxicity by modulating intrinsic self-assembly. *Proc. Natl. Acad. Sci. USA* **2018**, *115*, E10495–E10504. [[CrossRef](#)]
- Renaud, L.; Picher-Martel, V.; Codron, P.; Julien, J.P. Key role of UBQLN2 in pathogenesis of amyotrophic lateral sclerosis and frontotemporal dementia. *Acta Neuropathol. Commun.* **2019**, *7*, 103. [[CrossRef](#)] [[PubMed](#)]
- Yang, H.; Yue, H.W.; He, W.T.; Hong, J.Y.; Jiang, L.L.; Hu, H.Y. PolyQ-expanded huntingtin and ataxin-3 sequester ubiquitin adaptors hHR23B and UBQLN2 into aggregates via conjugated ubiquitin. *FASEB J.* **2018**, *32*, 2923–2933. [[CrossRef](#)] [[PubMed](#)]
- Yasuda, S.; Tsuchiya, H.; Kaiho, A.; Guo, Q.; Ikeuchi, K.; Endo, A.; Arai, N.; Ohtake, F.; Murata, S.; Inada, T.; et al. Stress- and ubiquitylation-dependent phase separation of the proteasome. *Nature* **2020**, *578*, 296–300. [[CrossRef](#)]
- Mueller, T.D.; Kamionka, M.; Feigon, J. Specificity of the interaction between ubiquitin-associated domains and ubiquitin. *J. Biol. Chem.* **2004**, *279*, 11926–11936. [[CrossRef](#)]
- Zhang, D.; Raasi, S.; Fushman, D. Affinity makes the difference: Nonselective interaction of the UBA domain of Ubiquilin-1 with monomeric ubiquitin and polyubiquitin chains. *J. Mol. Biol.* **2008**, *377*, 162–180. [[CrossRef](#)]
- Swatek, K.N.; Komander, D. Ubiquitin modifications. *Cell Res.* **2016**, *26*, 399–422. [[CrossRef](#)] [[PubMed](#)]
- Koyano, F.; Okatsu, K.; Kosako, H.; Tamura, Y.; Go, E.; Kimura, M.; Kimura, Y.; Tsuchiya, H.; Yoshihara, H.; Hirokawa, T.; et al. Ubiquitin is phosphorylated by PINK1 to activate parkin. *Nature* **2014**, *510*, 162–166. [[CrossRef](#)] [[PubMed](#)]
- Ye, S.X.; Gong, Z.; Yang, J.; An, Y.X.; Liu, Z.; Zhao, Q.; Lescop, E.; Dong, X.; Tang, C. Ubiquitin is double-phosphorylated by PINK1 for enhanced pH-sensitivity of conformational switch. *Protein Cell* **2019**, *10*, 908–913. [[CrossRef](#)]
- Tang, C.; Zhang, W.P. How Phosphorylation by PINK1 Remodels the Ubiquitin System: A Perspective from Structure and Dynamics. *Biochemistry* **2020**, *59*, 26–33. [[CrossRef](#)] [[PubMed](#)]
- Matsuda, N.; Sato, S.; Shiba, K.; Okatsu, K.; Saisho, K.; Gautier, C.A.; Sou, Y.S.; Saiki, S.; Kawajiri, S.; Sato, F.; et al. PINK1 stabilized by mitochondrial depolarization recruits Parkin to damaged mitochondria and activates latent Parkin for mitophagy. *J. Cell Biol.* **2010**, *189*, 211–221. [[CrossRef](#)]
- Gladkova, C.; Maslen, S.L.; Skehel, J.M.; Komander, D. Mechanism of parkin activation by PINK1. *Nature* **2018**, *559*, 410–414. [[CrossRef](#)]
- Fiesel, F.C.; Ando, M.; Hudec, R.; Hill, A.R.; Castanedes-Casey, M.; Caulfield, T.R.; Moussaoud-Lamodièrè, E.L.; Stankowski, J.N.; Bauer, P.O.; Lorenzo-Betancor, O.; et al. (Patho-)physiological relevance of PINK1-dependent ubiquitin phosphorylation. *EMBO Rep.* **2015**, *16*, 1114–1130. [[CrossRef](#)] [[PubMed](#)]
- Hou, X.; Fiesel, F.C.; Truban, D.; Castanedes Casey, M.; Lin, W.L.; Soto, A.I.; Tacic, P.; Rousseau, L.G.; Diehl, N.N.; Heckman, M.G.; et al. Age- and disease-dependent increase of the mitophagy marker phospho-ubiquitin in normal aging and Lewy body disease. *Autophagy* **2018**, *14*, 1404–1418. [[CrossRef](#)]

20. Wauer, T.; Swatek, K.N.; Wagstaff, J.L.; Gladkova, C.; Pruneda, J.N.; Michel, M.A.; Gersch, M.; Johnson, C.M.; Freund, S.M.; Komander, D. Ubiquitin Ser65 phosphorylation affects ubiquitin structure, chain assembly and hydrolysis. *EMBO J.* **2015**, *34*, 307–325. [[CrossRef](#)]
21. Swaney, D.L.; Rodriguez-Mias, R.A.; Villen, J. Phosphorylation of ubiquitin at Ser65 affects its polymerization, targets, and proteome-wide turnover. *EMBO Rep.* **2015**, *16*, 1131–1144. [[CrossRef](#)]
22. Huguenin-Dezot, N.; De Cesare, V.; Peltier, J.; Knebel, A.; Kristaryianto, Y.A.; Rogerson, D.T.; Kulathu, Y.; Trost, M.; Chin, J.W. Synthesis of Isomeric Phosphoubiquitin Chains Reveals that Phosphorylation Controls Deubiquitinase Activity and Specificity. *Cell Rep.* **2016**, *16*, 1180–1193. [[CrossRef](#)]
23. Wauer, T.; Simicek, M.; Schubert, A.; Komander, D. Mechanism of phospho-ubiquitin-induced PARKIN activation. *Nature* **2015**, *524*, 370–374. [[CrossRef](#)] [[PubMed](#)]
24. Dong, X.; Gong, Z.; Lu, Y.B.; Liu, K.; Qin, L.-Y.; Ran, M.L.; Zhang, C.L.; Liu, Z.; Zhang, W.P.; Tang, C. Ubiquitin S65 phosphorylation engenders a pH-sensitive conformational switch. *Proc. Natl. Acad. Sci. USA* **2017**, *114*, 6770–6775. [[CrossRef](#)] [[PubMed](#)]
25. Kazansky, Y.; Lai, M.Y.; Singh, R.K.; Fushman, D. Impact of different ionization states of phosphorylated Serine-65 on ubiquitin structure and interactions. *Sci. Rep.* **2018**, *8*, 2651. [[CrossRef](#)]
26. Delaglio, F.; Grzesiek, S.; Vuister, G.W.; Zhu, G.; Pfeifer, J.; Bax, A. NMRPipe: A multidimensional spectral processing system based on UNIX pipes. *J. Biomol. NMR* **1995**, *6*, 277–293. [[CrossRef](#)]
27. Vranken, W.F.; Boucher, W.; Stevens, T.J.; Fogh, R.H.; Pajon, A.; Llinas, M.; Ulrich, E.L.; Markley, J.L.; Ionides, J.; Laue, E.D. The CCPN data model for NMR spectroscopy: Development of a software pipeline. *Proteins* **2005**, *59*, 687–696. [[CrossRef](#)]
28. Mittermaier, A.; Kay, L.E. New tools provide new insights in NMR studies of protein dynamics. *Science* **2006**, *312*, 224–228. [[CrossRef](#)] [[PubMed](#)]
29. Sugase, K.; Konuma, T.; Lansing, J.C.; Wright, P.E. Fast and accurate fitting of relaxation dispersion data using the flexible software package GLOVE. *J. Biomol. NMR* **2013**, *56*, 275–283. [[CrossRef](#)] [[PubMed](#)]
30. Latham, M.P.; Zimmermann, G.R.; Pardi, A. NMR chemical exchange as a probe for ligand-binding kinetics in a theophylline-binding RNA aptamer. *J. Am. Chem. Soc.* **2009**, *131*, 5052–5053. [[CrossRef](#)]
31. Rückert, M.; Otting, G. Alignment of biological macromolecules in novel nonionic liquid crystalline media for NMR experiments. *J. Am. Chem. Soc.* **2000**, *122*, 7793–7797. [[CrossRef](#)]
32. Schwieters, C.D.; Bermejo, G.A.; Clore, G.M. Xplor-NIH for molecular structure determination from NMR and other data sources. *Protein Sci.* **2018**, *27*, 26–40. [[CrossRef](#)] [[PubMed](#)]
33. Jiang, W.X.; Gu, X.H.; Dong, X.; Tang, C. Lanthanoid tagging via an unnatural amino acid for protein structure characterization. *J. Biomol. NMR* **2017**, *67*, 273–282. [[CrossRef](#)] [[PubMed](#)]
34. Massi, F.; Grey, M.J.; Palmer, A.G., 3rd. Microsecond timescale backbone conformational dynamics in ubiquitin studied with NMR R1rho relaxation experiments. *Protein Sci.* **2005**, *14*, 735–742. [[CrossRef](#)]
35. Lange, O.F.; Lakomek, N.A.; Fares, C.; Schroder, G.F.; Walter, K.F.; Becker, S.; Meiler, J.; Grubmuller, H.; Griesinger, C.; de Groot, B.L. Recognition dynamics up to microseconds revealed from an RDC-derived ubiquitin ensemble in solution. *Science* **2008**, *320*, 1471–1475. [[CrossRef](#)]
36. Ban, D.; Funk, M.; Gulich, R.; Egger, D.; Sabo, T.M.; Walter, K.F.; Fenwick, R.B.; Giller, K.; Pichierri, F.; de Groot, B.L.; et al. Kinetics of conformational sampling in ubiquitin. *Angew. Chem. Int. Ed. Engl.* **2011**, *50*, 11437–11440. [[CrossRef](#)]
37. Wlodarski, T.; Zagrovic, B. Conformational selection and induced fit mechanism underlie specificity in noncovalent interactions with ubiquitin. *Proc. Natl. Acad. Sci. USA* **2009**, *106*, 19346–19351. [[CrossRef](#)]
38. Peters, J.H.; de Groot, B.L. Ubiquitin dynamics in complexes reveal molecular recognition mechanisms beyond induced fit and conformational selection. *PLoS Comput. Biol.* **2012**, *8*, e1002704. [[CrossRef](#)]
39. Paul, F.; Weikl, T.R. How to Distinguish Conformational Selection and Induced Fit Based on Chemical Relaxation Rates. *PLoS Comput. Biol.* **2016**, *12*, e1005067. [[CrossRef](#)]
40. Phillips, A.H.; Zhang, Y.; Cunningham, C.N.; Zhou, L.; Forrest, W.F.; Liu, P.S.; Steffek, M.; Lee, J.; Tam, C.; Helgason, E.; et al. Conformational dynamics control ubiquitin-deubiquitinase interactions and influence in vivo signaling. *Proc. Natl. Acad. Sci. USA* **2013**, *110*, 11379–11384. [[CrossRef](#)]
41. Hammes, G.G.; Chang, Y.C.; Oas, T.G. Conformational selection or induced fit: A flux description of reaction mechanism. *Proc. Natl. Acad. Sci. USA* **2009**, *106*, 13737–13741. [[CrossRef](#)] [[PubMed](#)]
42. Vogt, A.D.; Di Cera, E. Conformational selection or induced fit? A critical appraisal of the kinetic mechanism. *Biochemistry* **2012**, *51*, 5894–5902. [[CrossRef](#)] [[PubMed](#)]